Available online at BCREC website: https://bcrec.id

Bulletin of Chemical Reaction Engineering & Catalysis, 17 (4) 2022, 683-698

Research Article

Phytochemical-assisted Synthesis of Titania Nanoparticles using Azadirachta indica Leaf Extract as Photocatalyst in the Photodegradation of Methyl Orange

Imad Eddine Aouissi[1], Sheela Chandren*[1,2], Norazah Basar[1], Wan Nazihah Wan Ibrahim[3]

[1]Department of Chemistry, Faculty of Science, Universiti Teknologi Malaysia, 81310 UTM Johor Bahru, Johor, Malaysia.
[2]Centre for Sustainable Nanomaterials, Ibnu Sina Institute for Scientific and Industrial Research, Universiti Teknologi Malaysia, 81310 UTM Johor Bahru, Johor, Malaysia.
[3]Faculty of Applied Sciences, Universiti Teknologi MARA, 40450 Shah Alam, Selangor, Malaysia.

Received: 18th August 2022; Revised: 25th September 2022; Accepted: 25th September 2022
Available online: 29th September 2022; Published regularly: December 2022

Abstract

The biosynthesis procedure for nanomaterial preparation is a promising alternative due to its simplicity and environmental friendliness. In this work, TiO_2 NPs were biosynthesized using the aqueous leaf extract of *Azadirachta indica*. The influence of the extract volumes, solvents, and acetic acid on the properties of TiO_2 NPs was studied. Phytochemical screening and ATR-FTIR spectrum confirmed the presence of phenolic compounds in the leaf extract. XRD patterns showed that the samples were mainly in the anatase phase. However, for the water-based samples and when 1 and 2 mL of extract volumes were used, anatase/brookite mixture was observed. FESEM images displayed almost spherical and agglomerated NPs. UV-Vis-NIR studies showed that the samples' bandgaps values are within the range of anatase TiO_2. The photocatalytic activity of the TiO_2 NPs was evaluated in the photodegradation of methyl orange (MO) under UV light irradiation. The water-based sample synthesized using 2 mL of the extract achieved 98.62% of MO degradation within 270 min and demonstrated the highest pseudo-first-order photodegradation kinetic constant of 0.0147 min^{-1}. These results indicate that the use of the plant-based biosynthesis method with water as the solvent successfully produced TiO_2 NPs with good physicochemical properties and photocatalytic activity in the photodegradation of organic dye.

Keywords: Biosynthesis; titania nanoparticles; Azadirachta indica; photocatalytic activity; photodegradation

How to Cite: I.E. Aouissi, S. Chandren, N. Basar, W.N.W. Ibrahim, (2022). Phytochemical-assisted Synthesis of Titania Nanoparticles using Azadirachta indica Leaf Extract as Photocatalyst in the Photodegradation of Methyl Orange. *Bulletin of Chemical Reaction Engineering & Catalysis*, 17(4), 683-698 (doi: 10.9767/bcrec.17.4.15581.683-698)

Permalink/DOI: https://doi.org/10.9767/bcrec.17.4.15581.683-698

1. Introduction

In recent decades, nanotechnology has undergone a rapid evolution, mainly thanks to the development of nanoparticles (NPs), which have various applications in science and technology [1]. At present, the use of NPs is gaining widespread interest [1] as it has been observed that material properties are enhanced with decreasing size. For example, the physicochemical, magnetic, optical, distribution, and morphological properties are significantly improved when compared to materials of larger sizes [2]. NPs have been extensively utilized in medicine, domestic water purification systems, cosmetics, electronics, solar panels, textiles, sensor tech-

* Corresponding Author.
Email: sheela@utm.my (S. Chandren)

nology, industrial applications, commercial products, environmental sanitation, and biomedical equipment [3].

The synthesis of NPs can be achieved by various chemical, physical, or biological methods [4]. A new branch termed nanobiotechnology was recently proposed; the melding of nanotechnological advancement with principles of biotechnology by combining physical and chemical techniques to synthesize NPs, serving a specific application [5]. Nanobiotechnology is seen as a promising branch due to the overwhelming potential for healthy, eco-friendly, and hygienic methods for metallic NPs synthesis [6].

Chemical and physical synthesis methods require a significant amount of hazardous chemicals, which are not environmentally friendly and can be detrimental to humans. In addition to the sizeable use of harmful chemicals, these synthesis methods are costly and require a considerable amount of heat and pressure [7,8]. Toxic chemicals can limit this material's advantages in some possible medical applications, as some chemical species are adsorbed onto the particles' surface [9, 10]. Apart from toxicity, scientists face difficulties in controlling the size and shape as well as achieving the monodispersity of NPs [11]. Therefore, such methods must be replaced with a feasible method that mitigates these issues.

Among the known preparation methods, the biosynthesis method emerges as the most favorable. Aside from limiting the use of harmful solvents and surfactants, it is considered an improved approach used to produce self-aggregated, well-defined morphology, controlled shape, and size NPs [12,13]. In addition, it does not require high pressure or high temperature, and above all, it is not harmful to the environment [14]. Plants, bacteria, fungi, algae, and actinomycetes can all be used to produce NPs, and have been proven to improve the photocatalytic and pharmacological characteristics of the synthesized NPs [15]. According to Nadeem *et al.* [16], plants, particularly the leaves, are the most suitable for NPs synthesis because they are rich in metabolites, which are mainly involved in the reduction process. The leaves of plants have been found to contain useful phytochemicals, such as ketones, aldehydes, flavones, amides, terpenoids, carboxylic acids, phenols, and ascorbic acids, which can serve as reducing and capping agents for NPs [17]. Compared to employing microorganisms, which need delicate conditions, such as pH and temperature, for the preservation and other requirements for microbial growth, using phytochemicals is simple, easy, cost-effective, and delivers a high yield while preserving sustainable developments [18]. It has been reported in the literature that phytochemicals may also play a role in photocatalytic activity applications. In fact, they participate in oxidation and reduction reactions during the photocatalytic activity of organic dyes [19].

The properties of titania (TiO_2), such as its high photocatalytic activity, exceptional physical and chemical stability, low cost, non-corrosive, nontoxicity, and high availability, have made it the focus of numerous studies in comparison to other materials [20]. Generally, the synthesis of TiO_2 gives crystalline and amorphous forms and occurs mainly in three polymorphic crystalline forms: brookite, rutile, and anatase [21]. TiO_2 has been explored in various applications, including water purification [22], biotechnology such as cosmetics, medicines, and pharmaceutical products [23, 24], hydrogen production through water splitting [25], and various others. In wastewater issues and treatment, methyl orange (MO) dye is a common industrially produced azo dye that can generate a considerable amount of coloured wastewater if discharged into the wastewater system. The traditional biological, physical, or chemical treatments face limitations in dye wastewater treatment [26,27]. On the contrary, photocatalytic technology is one of the most appropriate techniques for azo dyes reduction dyes [28]. It can fundamentally eliminate contaminants relative to the conventional wastewater treatment process, and despite the liquid or gaseous state of the pollutants, photocatalytic technology can have a good degradation effect [29]. The fact that TiO_2 NPs absorb 3 – 4% of solar energy makes them the most effective solar collector [19], and therefore, they are well-known photocatalysts for the decomposition of hazardous chemical compounds in water [30]. In recent years, several studies have reported on the synthesis of TiO_2 NPs facilitated by plant-based extracts, including *Trigonella foenum-graecum* [31], *Cinnamomum zeylanicum* [30], *Carica papaya* [32], *Cucurbita pepo* [33], *Justicia gendarussa* [34], *Matricaria chamomilla* [35], *Thymus migricus* and *Alcea* [36], *Tamarindus indica* [37], *Punica granatum*, *Lippia citriodora* [38], *Deinbollia pinnata* [15], and *Prunus domestica L.* [5].

Azadirachta indica or neem (*A. indica*) plant is a species of the Meliaceae family and, while commonplace in India, can also be found

in other south-east Asian countries [39,40], including Malaysia [41]. *A. indica* is well-known for its various advantageous properties, such as anti-inflammatory, antioxidant, antifungal, antidiabetic, anticancer, antiviral, and other activities [42,43]. Several compounds in *A. indica* leaves have been shown to be favorable for the synthesis of TiO_2 NPs, such as flavonoids, polyphenols, alkaloids, and terpenoid compounds [44]. To the best of our knowledge, only a small number of works have been reported on the use of *A. indica*, especially the leaves. Among these, some have been done on the synthesis of ZnO [45], Ag [46], and TiO_2 [47]. In the current study, a more comprehensive work that outlines the potential mechanism for the biosynthesis of TiO_2 NPs and identifies the potentially responsible compounds is presented. Moreover, the TiO_2 biosynthesis method using *A. Indica* leaves have various synthesis parameters that have not been examined in previous works. Therefore, getting a deeper understanding of these parameters is greatly beneficial to the development of the biosynthesis method. In this work, TiO_2 NPs have been synthesized using an aqueous extract of *A. Indica* and influencing parameters, such as the volume of plant extract, solvents, and the influence of glacial acetic acid, on the properties of TiO_2 NPs were studied, followed by the evaluation of the photocatalytic activity. The synthesis procedure used in this work is inspired by a study reported by Senthilkumar and Rajendran [34].

2. Materials and Methods

2.1 Materials

The plant leaves of *A. indica* were collected from Johor Bahru, Johor, a state in the south of Malaysia. Ferric chloride ($FeCl_3$, (97%)), sodium hydroxide (NaOH, (98%)), hydrochloric acid (HCl, (37%)), chloroform ($CHCl_3$, (99%)), and sulfuric acid (H_2SO_4, (98%)) were purchased from Sigma-Aldrich and used for the leaf extract phytochemical screening tests. Titanium tetra-isopropoxide (TTIP) (C_{12}-$H_{28}O_4Ti$, Sigma-Aldrich (97%)), ethanol absolute (C_2H_6O, MERK (99.9%)), and glacial acetic acid (CH_3COOH, HmbG (99%)) were used for TiO_2 NPs preparation. The photocatalytic activity of the biosynthesized TiO_2 NPs was evaluated in the photodegradation of methyl orange (MO) ($C_{14}H_{14}N_3NaO_3S$, Sigma-Aldrich (85%)). A commercial TiO_2 (Anatase, <25 nm particle size, spec. the surface area of 45 – 55 m^2/g, Sigma-Aldrich (99.7%)) was purchased in order to compare its photodegradation efficiency with the biosynthesized TiO_2 NPs. All the chemicals were used as received without further purification.

2.2. Preparation of *A. indica* Leaf Extract

Fresh and healthy leaves of *A. indica* leaves were collected, and the impurities or dust on the leaves were removed with tap water followed by distilled water. The leaves were then left to dry for 14 days at room temperature to remove any moisture residue. They were further cut into pieces and ground using a mixer grinder. About 20 g of finely cut *A. indica* leaves were placed in a beaker containing 100 mL of distilled water. The content was mixed thoroughly and heated at a constant temperature of 60 °C for 30 min in a water bath, with occasional stirring. The aqueous extract solution was later filtered through the Buchner funnel, which was equipped with a Whatman No.1 filter paper, connected to a vacuum pump, and then stored in a refrigerator at 4 °C.

2.3. Qualitative Phytochemical Screening of the Extract

The *A. indica* aqueous extract was subjected to chemical tests for the identification of its active constituents. The test was conducted using the methods reported by Vimalkumar *et al.* [48] and Bouasla *et al*. [49] with slight modifications. A 50% aqueous plant extract was prepared by adding 10 mL of the extract into a 20 mL volumetric flask, to which distilled water was added until reaching the mark. The prepared solution was used throughout the tests. Qualitative phytochemical analysis on the detection of phenol, flavonoid, and terpenoid was accomplished by using well-established standard methods. All these qualitative determinations rely on the visual colour change reaction as a basic response to the presence of a specific phytochemical compound in the extracts [50].

2.3.1. Detection of phenols

The test was conducted following the ferric chloride test by adding 2 mL of $FeCl_3$ (5%) to 2 mL of the extract. The formation of blue or black colour indicates the presence of phenols.

2.3.2. Detection of flavonoids

The detection of flavonoids was performed using the alkaline reagent test, where 2 mL of NaOH (2% w/v) was added to 2 mL of the extract, which will result in a colour change to deep yellow. A few drops of HCl (2 M) were then added, and the decolourisation of the yel-

low colour will serve as the indication of flavonoids' presence in the extract.

2.3.3. Detection of terpenoids

The Salkowski test was used for terpenoid detection. Around 2 mL of $CHCl_3$ was added to 2 mL of the extract, and two separate layers will be formed. Then, a few drops of concentrated H_2SO_4 were slowly added. The formation of a brick red colour between the layers will indicate the presence of terpenoids.

2.4. Synthesis of TiO_2 NPs

TiO_2 NPs were prepared by dissolving 14.8 mL of TTIP in 35.2 mL of water as the solvent and stirred for 10 min at room temperature. Then, a selected amount of the aqueous leaf extract (1, 2, 5, 10, and 15 mL) was added dropwise under continuous stirring for 1 h at room temperature. The resulting mixture was then treated with 10 min of ultrasound homogeniser (40% amplitude, 20 kHz frequency) and kept cold using an ice bath. Subsequently, hydrothermal treatment was applied to the mixture using stainless steel autoclave with a Teflon chamber and heated for 12 h at 180 °C. After cooling down the autoclave, the precipitate was washed with ethanol and centrifuged at 4000 rpm for 30 min three times before being put to dry at 60 °C for 16 h. After drying, the sample was calcined at 500 °C for 5 h. TiO_2 NPs were tested for their photocatalytic activity, and the collected data were contemplated as a base for subsequent synthesis.

Following the same steps described above, another sample was prepared by dissolving TTIP in ethanol absolute as the solvent instead of water. The influence of acetic acid was also studied by preparing two samples, where TTIP was dissolved in the selected solvent (ethanol or water), followed by the addition of leaf extract. However, prior to the ultrasound treatment, 5 mL of glacial acetic acid was slowly added to the mixture. Finally, a sample was prepared by a combinatorial approach, which consists of dissolving TTIP in a water-ethanol mixture at a volume ratio of 1:1 (17.6 mL each), and then aqueous leaf extracts and 5 mL of glacial acetic acid were slowly added. Table 1 lists the abbreviations for all the prepared samples.

2.5. Catalysts Characterisations

The X-ray diffraction (XRD) analysis was performed using an X-ray diffractometer (Rigaku Smart Lab, Japan) with Cu Kα radiation (λ=1.5418 Å, 40 kV, 30 mA), and the data was collected over 2θ ranging from 20 to 80 º. Fourier transform infrared (FTIR) spectra of the TiO_2 NPs using Perkin Elmer Spectrum 1600 FTIR spectrometer within the range from 4000 to 400 cm^{-1}. The functional groups present in the aqueous leaf extract were recorded by FTIR coupled with Attenuated total reflectance (ATR). Absorbance studies were recorded within the scope of 300 − 800 nm using Ultraviolet-Visible-Near-Infrared (UV-vis-NIR) spectrophotometer (SHIMADZU UV-3600Plus series). The specific surface area and pore size distribution studies were measured by nitrogen adsorption isotherms using Thermo Scientific Surfer Analyzer. The Brunauer-Emmett-Teller (BET) and Barrett–Joyner–Halenda (BJH) models were used to estimate the surface area and pore size of the TiO_2 NPs. The surface morphology was determined using a Field-emission scanning electron microscope (FESEM) (Zeiss Crossbeam 340).

2.6. Photocatalytic Activity of TiO_2 NPs

The photocatalytic activity was investigated by suspending 0.1 g of the prepared TiO_2 NPs

Table 1. List of samples abbreviations.

Sample	Abbreviations
TiO_2 was prepared with distilled water as the solvent and different amounts of leaf extracts, where the number at the back stands for the volume of extracts used.	TiO_2-DW-1, TiO_2-DW-2, TiO_2-DW-5, TiO_2-DW-10, and TiO_2-DW-15.
TiO_2 was prepared using ethanol as solvent.	TiO_2-EtOH
TiO_2 was prepared with the addition of acetic acid and distilled water as solvent.	TiO_2-DW-AA
TiO_2 was prepared with the addition of acetic acid and ethanol as solvent.	TiO_2-EtOH-AA
TiO_2 was prepared by combining solvents and acetic acid.	TiO_2-Comb

in a beaker containing 50 mL of MO dye solution (20 mg/L). The mixture was subjected to sonication to achieve homogeneity. The TiO_2 NPs and MO solution was kept in the dark under constant stirring for 1 h to reach adsorption equilibrium. The photocatalytic activity was then tested in the degradation of MO using a 6-watt UV lamp. During the reaction, 3 mL aliquot was taken after intervals of 30, 60, 90, 120, 150, 180, 210, 240, and 270 min (for 4.5 h). The obtained aliquots were subjected to centrifugation at 4000 rpm for 25 min and analysed using a Shimadzu UV-Vis spectrophotometer (UV-1800 240V, Japan). The dye concentration (%C) after various time intervals was calculated using the following Equation (1).

$$\%C = \frac{A_0 - A_t}{A_0} x100 \quad (1)$$

where, A_o and A_t are the absorbance of the dye before degradation and after degradation of dye at different time intervals time "*t*", respectively. Moreover, according to Dash *et al.* [51] , the kinetics of photocatalytic reactions are commonly investigated via the Pseudo-first-order rate law; therefore, the kinetics of MO dye degradation were investigated by employing the pseudo-first-order kinetics reaction and expressed by the integrated formula shown in Equation (2).

$$\ln \frac{A_0}{A_t} = kt \quad (2)$$

where, A_o is the initial absorbance of MO, A_t is the MO absorbance at a specific time (*t*), and *k* is the pseudo-first-order rate constant.

3. Results and Discussion

3.1. Phytochemical Screening Results

The results were based on the colour changes observed during the qualitative tests, as shown in Table 2. For the detection of the presence of phenolics, after the addition of $FeCl_3$, the colour changed to black, confirming the presence of phenolics. For the flavonoids test, when NaOH was added, the colour changed to a deep yellow colour, and once HCl solution was added, the colour started to get lighter. Based on these colour changes, it could be confirmed that flavonoids were present. As for the terpenoids detection test, two layers were formed after the addition of chloroform. However, when H_2SO_4 was added, the brick red colour did not appear between the two layers, showing no sign of terpenoids in the *A. indica* leaf extract.

Table 2. Phytochemical constituents present in *A. indica* leaf extract

Test	Constituents	Results
Ferric chloride test	Phenolics	Present
Alkaline reagent test	Flavonoids	Present
The Salkowski test	Terpenoids	Absent

3.2. Possible Mechanism for the Formation of TiO_2 NPs

Based on the phytochemical screening of *A. indica* leaf extract, the flavonoids and phenols are present and were reported to be the key bioreduction components in plant extracts. Similar studies on TiO_2 NPs biosynthesis using *A. indica* have suggested that these compounds have helped form and stabilize TiO_2 NPs with their ability to donate hydrogen atoms or electrons [18,47]. The mechanism of TiO_2 synthesis from TTIP ($Ti\{OCH(CH_3)_2\}_4$) precursor starts with the hydrolysis of TTIP by water molecules resulting in titanium hydroxide ($Ti(OH)_4$) as shown in the following Equation (3).

$$Ti[OCH(CH_3)_2]_4 + 4H_2O \rightarrow Ti(OH)_4 + 4(CH_3)_2CHOH \quad (3)$$

Previous research has shown that the leaves of *A. indica* produce polyphenolic flavonoids such as quercetin [52]. The hydrogen atom in each of the hydroxyl groups in quercetin initially acquires a partial charge by virtue of being attached to the highly electronegative oxygen atom, which hereby acquires a negative charge. Meanwhile, the hydroxide group attached to the titanium atom behaves in a similar fashion in which the oxygen and hydrogen atoms acquire a partial negative and positive charge, respectively. Due to the presence of lone pair electrons on the oxygen atom in the titanium complex, it pulls the positively charged hydrogen from the quercetin, generating an intermediate structure. The intermediate complex removes a water molecule from the titanium atom, leaving a positive charge on the atom, resulting in the positively charged $TiO(OH)_2$ intermediate. Figure 1 is the suggested bioreduction mechanism of TiO_2 NPs, similar to that proposed by Aslam *et al.* [53]. A similar process of electron transfer in the subsequent step results in the formation of the desired TiO_2 NPs.

3.3 Physicochemical Properties of TiO_2 NPs

3.3.1 Functional group analysis of *A. indica* leaf extract and TiO_2 NPs

FTIR spectroscopy was used to identify the functional groups present in the aqueous leaf extract of *A. indica* and the prepared TiO_2 NPs. The FTIR-ATR spectrum for the aqueous leaf extract is shown in Figure 2. The peak at 3300 cm^{-1} is associated with the OH band stretching vibration, which indicates the presence of alcohols and phenolic compounds. The vibrations of the C=C group of alkenes are denoted by the peak at 2073.56 cm^{-1}, while the C=O stretching of primary amides or the C=C groups of aromatic rings can be assigned to the peak at 1634 cm^{-1}. Meanwhile, the nitro N–O bending vibration is responsible for the peak at 1396 cm^{-1}, and the C–O vibrations of carboxylic acids peak can be seen at 1082 cm^{-1}. As reported by other research, the findings showed that flavonoids and proteins included in the extract are thought to be important for the formation and stabilization of TiO_2 NPs [18].

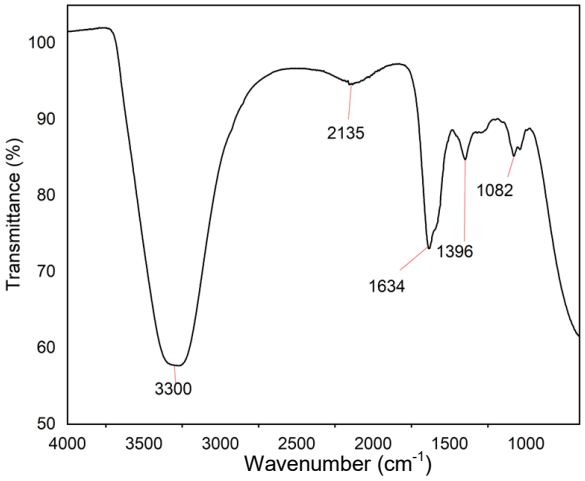

Figure 2. FTIR-ATR spectrum of aqueous *A. indica* leaf extract

Figure 3 shows the FTIR spectra of the biosynthesized TiO_2 NPs. The broad absorption bands observed at 3444 cm^{-1} and 1630 cm^{-1} correspond to the O–H bond stretching and bending vibrations at the surface of TiO_2 NPs, respectively, due to adsorbed moisture [51]. A broad absorption band in the region of 430 – 850 cm^{-1} is attributed to the Ti–O and Ti–O–O stretching vibrations in the TiO_2 NPs, confirming that TiO_2 NPs were successfully obtained [54,55]. The TiO_2 NPs calcined at 500 °C indicated no traces of organic components' functional groups, confirming complete calcination.

3.3.2 Crystallinity studies of TiO_2 NPs by X-ray diffraction

The crystallinity of the biosynthesized TiO_2 NPs was determined using XRD analysis. Figure 4 shows the XRD patterns of TiO_2-DW-1, TiO_2-DW-2, TiO_2-DW-5, TiO_2-DW-10, and TiO_2-DW-15. Within the 2θ range of 20 – 80 °, several diffraction peaks of the anatase phase (JCPDS no. 00-021-1272) were observed. The major peaks were observed at 2θ values of 25.31 °, 37.68 °, 48.02 °, 53.99 °, 55.03 °, 62.57 °, and 74.97 °, corresponding to (101), (004), (002), (105), (211), (204), and (215), respectively. However, a small amount of brookite phase (JCPDS no. 01-072-0100) was observed at a 2θ

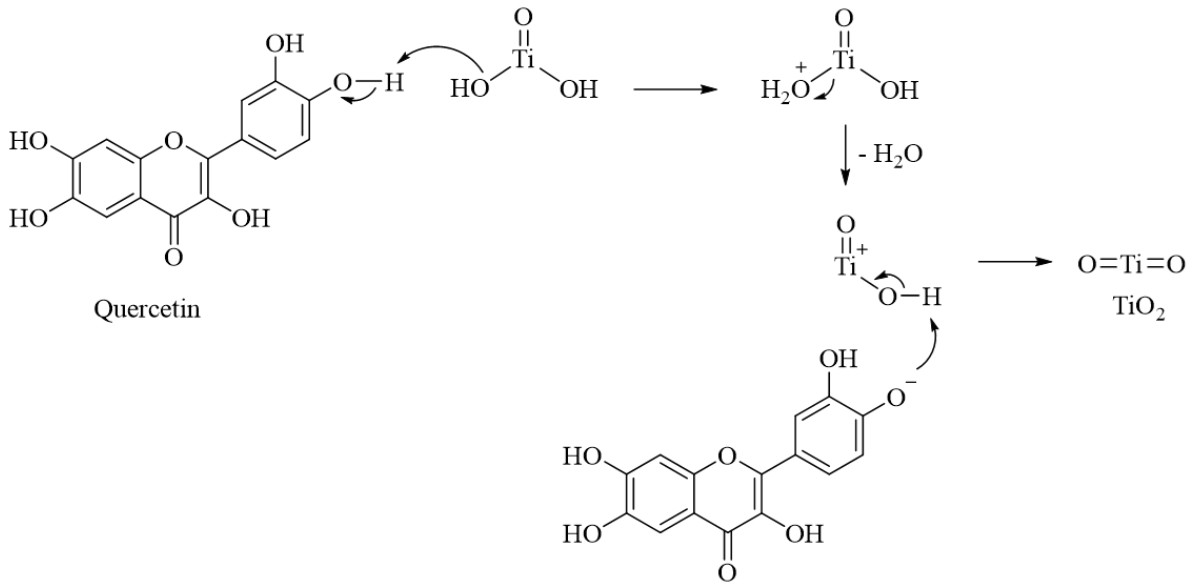

Figure 1. The possible mechanism of the bioreduction to TiO_2 NPs in the presence of quercetin in *A. indica* leaf extract

value of 30.81 ° corresponding to (211) for TiO_2-DW-1 and TiO_2-DW-2, with 12.0 and 3.1% of brookite phase, respectively. The anatase phase TiO_2 is thought to be the most active [56]. Nevertheless, it has been reported that the photocatalytic activity of samples with a mixture of phases (anatase/rutile or anatase/brookite) is better than that of single-phase samples [57]. Thus, TiO_2-DW-1 and TiO_2-DW-2 have shown a great performance suggesting that the phase mixture is one of the possible photocatalytic activity enhancing factors.

Based on the photocatalytic activity testing results, which will be discussed in the following sections, 2 mL of leaf extract was chosen as the optimum amount. Figure 5 shows the XRD results of TiO_2-DW-2, TiO_2-DW-AA, TiO_2-EtOH, TiO_2-EtOH-AA, and TiO_2-Comb. It was apparent that all the samples obtained a single anatase phase, except for TiO_2-DW-2. The XRD peaks of the biosynthesized TiO_2 NPs show that the TiO_2-DW-2 sample has very low crystallinity as the peaks became broader and weaker in intensity, indicating a decrease in crystallinity. As for the TiO_2-DW-AA sample, prepared with the addition of acetic acid, the diffractogram shows sharper peaks with stronger intensity compared to that of TiO_2-DW-2, which was prepared without acetic acid.

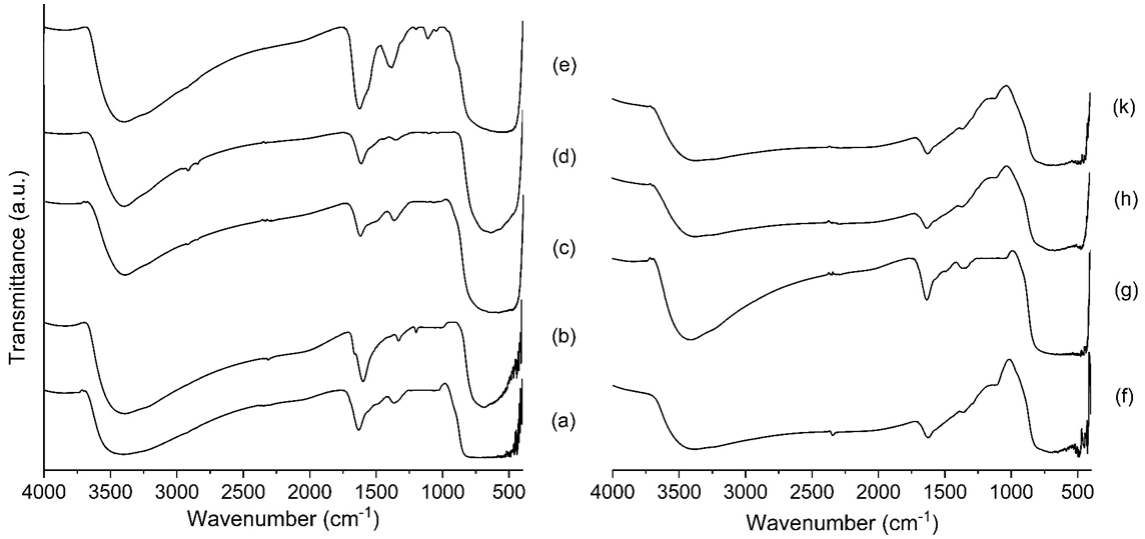

Figure 3. FTIR spectra of (a) TiO_2-DW-1, (b) TiO_2-DW-2, (c) TiO_2-DW-5, (d) TiO_2-DW-10, (e) TiO_2-DW-15 (f) TiO_2-DW-AA, (g) TiO_2-EtOH, (h) TiO_2-EtOH-AA, and (k), and TiO_2-Comb

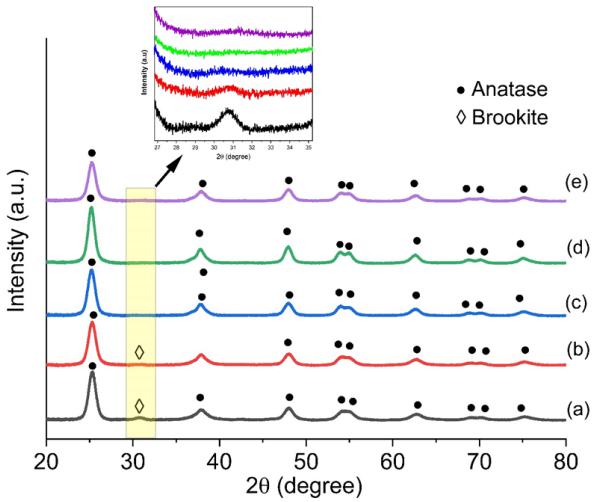

Figure 4. XRD patterns of the biosynthesized (a) TiO_2-DW-1, (b) TiO_2-DW-2, (c) TiO_2-DW-5, (d) TiO_2-DW-10, and (e) TiO_2-DW-15 samples, including an inset showing the zoomed-in view of brookite phase peak

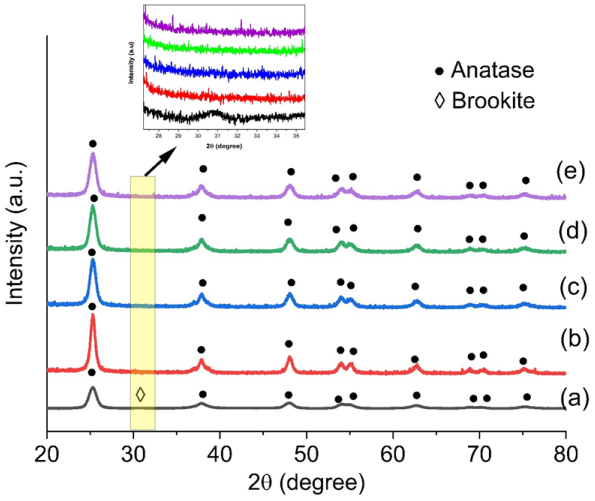

Figure 5. XRD patterns of (a) TiO_2-DW-2, (b) TiO_2-EtOH, (c) TiO_2-EtOH-AA, (d) TiO_2-DW-AA, and TiO_2-Comb samples, including an inset showing the zoomed-in view of brookite phase peak

This result is in agreement with the literature, which reported that the addition of acetic acid increases crystallinity [34]. TiO_2-EtOH shows the sharpest peaks with the strongest intensities, indicating its highest crystallinity than all of the prepared samples. The decrease in crystallinity for TiO_2-EtOH-AA and TiO_2-Comb could probably be due to the volume ratio of ethanol to acetic acid, which further decreased for the TiO_2-Comb sample. This may have affected the content of anatase produced in TiO_2 NPs [58]. Even though crystallinity is an important factor, there is no clear conclusion on the individual impact of crystallinity on photocatalytic activity [56]. This is because anatase NPs usually exhibit a broad distribution of crystallite sizes [59], where the photocatalytic activity can also be influenced by other physical properties [60], such as the NPs size and surface area.

3.3.3 Morphology of TiO_2 NPs by FESEM

The morphology of the TiO_2 NPs can be seen in the FESEM images shown in Figure 6. All the samples show agglomeration and are almost spherical in nature. The average particle sizes of TiO_2-EtOH, TiO_2-EtOH-AA, and TiO_2-Comb are 30.4, 27.4, and 27.3 nm, respectively; larger than TiO_2-DW-2 and TiO_2-DW-AA, both of which have smaller average particle sizes of 21.0 and 22.5 nm, respectively. This can potentially be linked to the polarity index of the reaction medium [61]. According to the author, the size of the NPs increases with the decrease in the polarity index. In this case, ethanol-

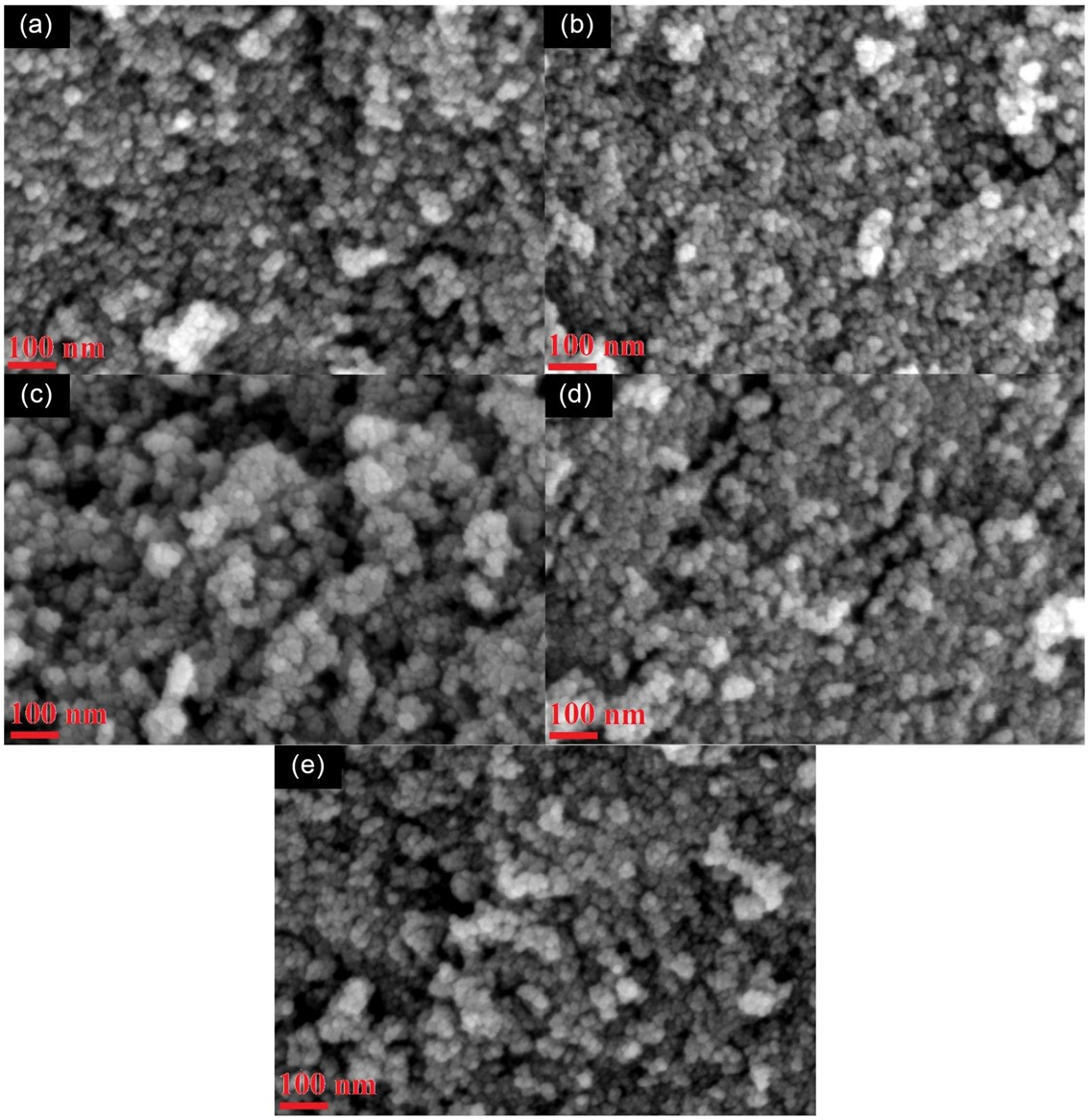

Figure 6. FESEM images of (a) TiO_2-DW-2, (b) TiO_2-DW-AA, (c) TiO_2-EtOH, (d) TiO_2-EtOH-AA, and (e) TiO_2-Comb, with magnification of 100000 times

based samples have resulted in larger sizes in comparison to water-based samples. In a medium with a high polarity index, a large number of charged ions are adsorbed on the surface of the NPs, leading to the formation of an electrical double layer around the colloidal particles [62]. This increases the particles' zeta potential, thereby preventing aggregation by repulsion. Control of the surface charge can be achieved by changing the solvent's polarity, which governs the interaction between particles leading to size control [63]. The optical, electronic, and catalytic characteristics of NPs are significantly influenced by their size and shape due to variations in surface area, the number of active sites, and the quantum size effect [64]. The small NPs size can cause an increase in their specific surface area, which can enhance the photocatalytic activity. The FESEM results have indicated that the biosynthesized TiO_2 NPs could be an effective way to obtain small-size TiO_2 NPs.

3.3.4 UV-Vis-NIR studies of TiO_2 NPs

The absorption spectra of TiO_2-EtOH, TiO_2-DW-2, TiO_2-DW-AA, TiO_2-Comb, and TiO_2-EtOH-AA are shown in Figure 7(a), wherein the absorption edge of the samples have estimated wavelength values of 365, 369, 374, 379, and 383 nm, respectively. TiO_2-DW-AA, TiO_2-EtOH-AA, and TiO_2-Comb samples show higher wavelength as their NPs sizes decreased compared to that of the TiO_2-EtOH sample, where the absorption edge was largely shifted to a lower wavelength. This is most likely due to the increase in particle size [65]. However, in the case of TiO_2-DW-2, the absorption edge shifted to a lower wavelength, possibly due to the presence of brookite, as it has been reported that anatase and brookite mixture would cause a blue shift in the wavelength [66].

The bandgap energy of the TiO_2 NPs was determined using the UV-Vis-NIR absorption spectra by utilizing the Tauc plot to plot $(ahn)^{1/2}$ vs. hn. Based on the value of the x-intercept, the bandgap energy of TiO_2 NPs was obtained by taking the linear extrapolation in the plot, as seen in Figure 7(b) – (f). The bandgap energy values of TiO_2-EtOH, TiO_2-DW-2, TiO_2-DW-AA, TiO_2-Comb, and TiO_2-EtOH-AA samples are 3.22, 3.18, 3.17, 3.16, and 3.14 eV, respectively. The TiO_2 NPs' bandgap energy values were in the range of the

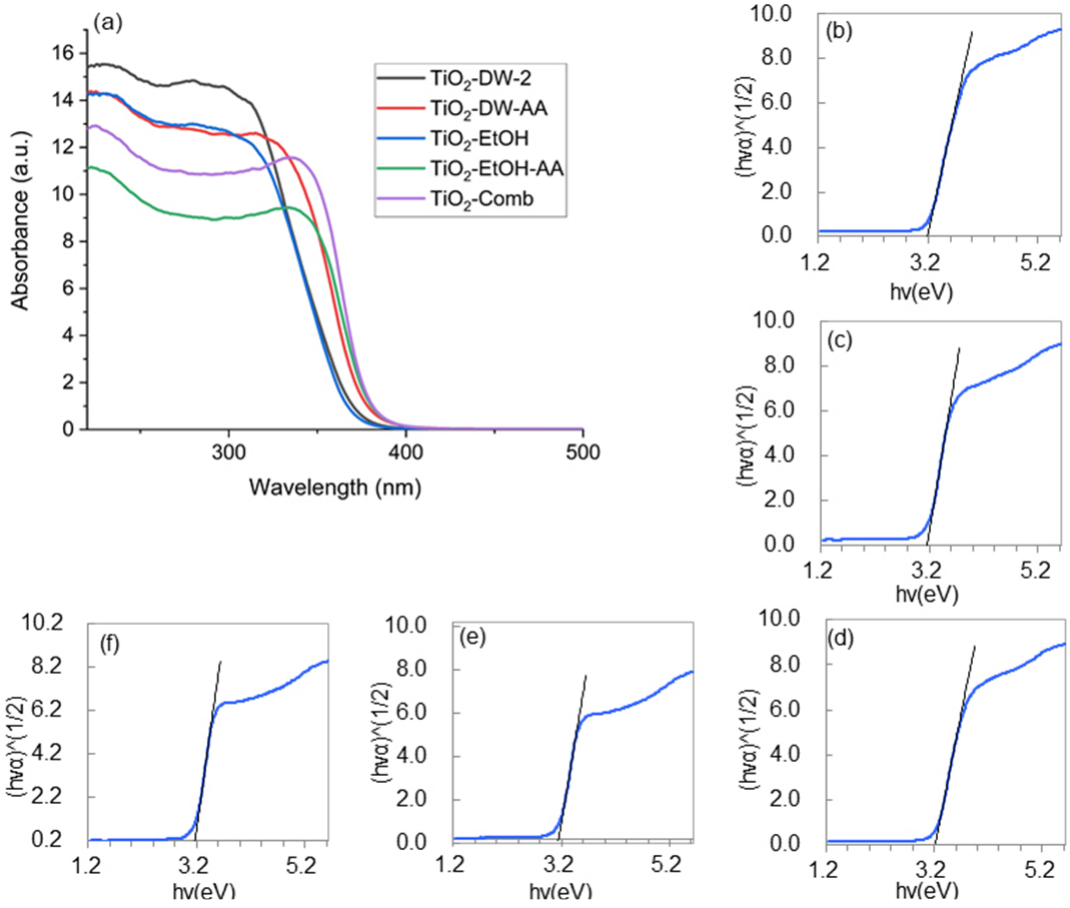

Figure 7. UV-Vis-NIR absorption spectra of (a) the prepared TiO_2 NPs combined and Tauc plots of (b) TiO_2-DW-2, (c) TiO_2-DW-AA, (d) TiO_2-EtOH, (e) TiO_2-EtOH-AA, and (f) TiO_2-Comb

anatase phase [67]. However, the bandgaps value variation can be due to factors such as the NPs size or the presence of phase mixtures in the case of the TiO_2-DW-2 sample having a small amount of brookite phase [57,68]. Therefore, the values are in agreement with the XRD results.

3.3.5 BET surface area and pore volume of TiO_2-NP

The adsorption-desorption isotherms of the prepared TiO_2 NPs are shown in Figure 8. All the isotherms are of Type IV, according to IUPAC's classification, which indicates the properties of mesoporous materials [69]. TiO_2-DW-AA, TiO_2-Comb, and TiO_2-EtOH-AA samples have the type H1 hysteresis loop. This means that the materials consist of an open, uniformly sized cylindrical pore [70]. The hysteresis loop assigned to TiO_2-DW-2 and TiO_2-EtOH samples are type H3, which indicates that the materials have aggregate slit-shaped pores [70]. The addition of acetic acid to the process is plausibly responsible for this difference. In a research published by Mahmoud *et al*. [71], acetic acid and other acid species were used to illustrate how they affect the physicochemical characteristics of TiO_2 NPs. The study also revealed how the hysteresis loops changed depending on the acid utilized. According to another study by Nguyen *et al*. [72], the type of acid employed and its quantity have an impact on the isotherm type. Therefore, in this study, the use of acetic acid in the process is a potential factor in the emergence of different hysteresis loop types.

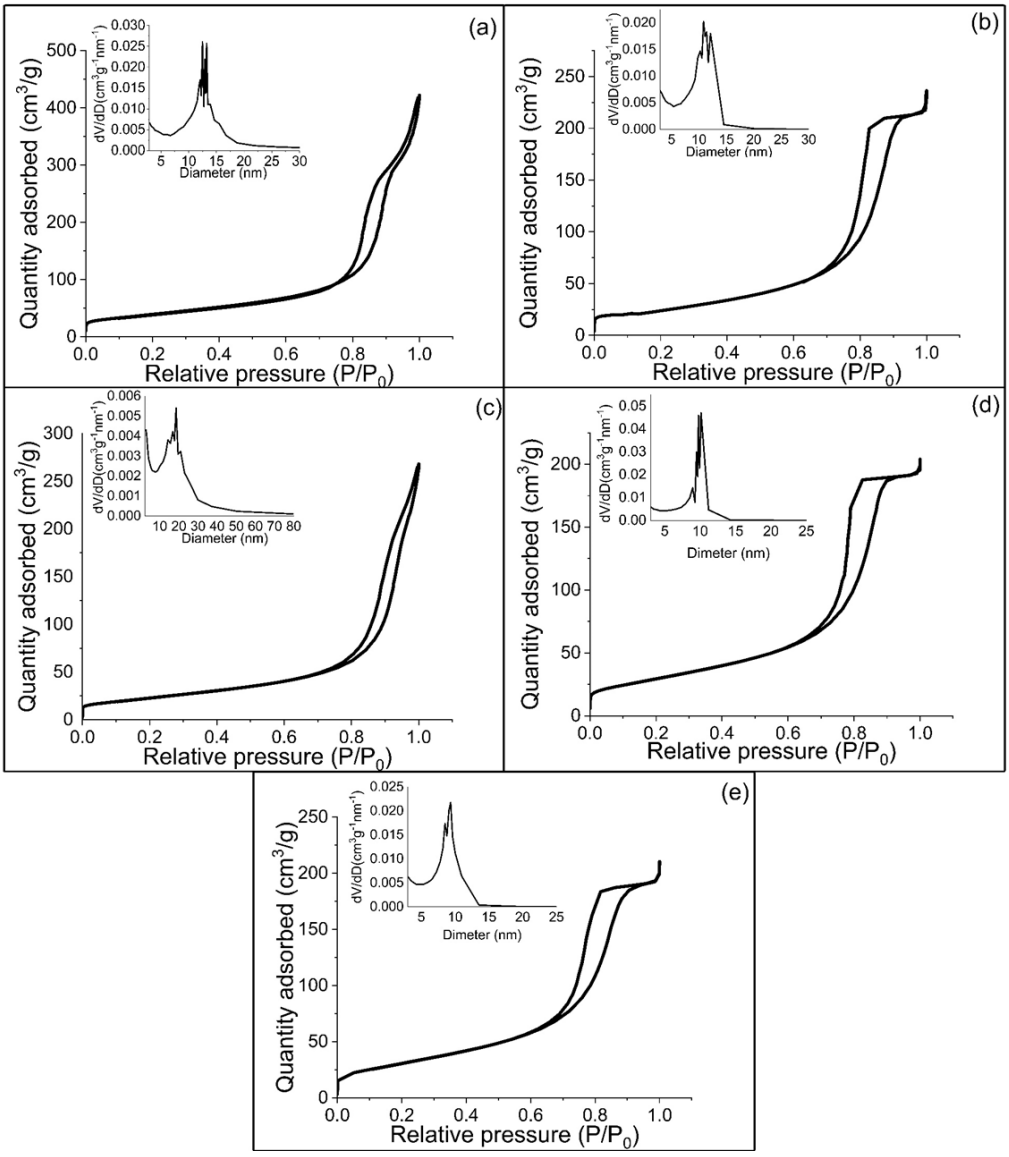

Figure 8. N_2 adsorption-desorption isotherms and pore size distribution (inset) of (a) TiO_2-DW-2, (b) TiO_2-DW-AA, (c) TiO_2-EtOH, (d) TiO_2-EtOH-AA, and (e) TiO_2-Comb

The distribution of TiO_2 NP's pore size was measured using the BJH method from the desorption branch, and the plots are shown in the inset of Figure 8. The samples' BET surface areas, average pore size distribution, and pore volumes are summarized in Table 3. Using the BJH method, the pore volumes of the biosynthesized TiO_2 NPs were calculated. Compared to all the other samples, TiO_2-DW-2 displayed a significantly higher surface area (144.0 m^2/g) and pore volume (0.6602 cm^3/g), which previous studies stated that the higher the surface area, pore sizes, and volumes are for mesoporous TiO_2, the more enhanced the photocatalytic activity of the material due to the access improvement to their active sites [73,74]. On the other hand, TiO_2-EtOH has the lowest surface area as it has the largest NPs sizes.

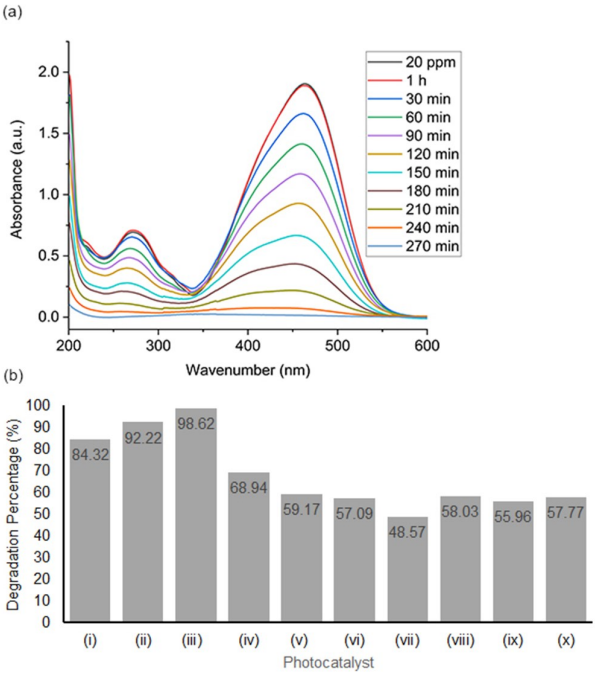

Figure 9. (a) The UV-Vis absorbance spectra of MO aqueous solution in the presence of TiO_2-DW-2, (b) Degradation percentages of MO dye solution in the presence of (i) TiO_2-Commercial, (ii) TiO_2-DW-1, (iii) TiO_2-DW-2, (iv) TiO_2-DW-5, (v) TiO_2-DW-10, (vi) TiO_2-DW-15, (vii) TiO_2-DW-AA, (viii) TiO_2-EtOH, (ix) TiO_2-EtOH-AA, and (x) TiO_2-Comb

3.4. Photocatalytic Activity of TiO_2 NPs

The photocatalytic activity of the biosynthesized TiO_2 NPs was tested in the photodegradation of MO dye under UV light irradiation. All of the samples were capable of degrading MO under UV light irradiation. The UV spectra of MO and TiO_2-DW-2 reaction under 1 h of dark condition and under UV light every 30 min within 270 min are shown in Figure 9(a) as an example of the degradation monitoring process. By comparing all the degradation percentages, as shown in Figure 9(b), TiO_2-DW-2 clearly demonstrated the best photocatalytic activity with an MO degradation percentage of 98.62% after 270 min. This is most likely due to the small particle sizes, resulting in a significantly higher surface area. This will, in turn, increase the photocatalytic activity of TiO_2 NPs [75]. Furthermore, as mentioned before, the mixture of anatase/brookite phases could have also improved the photocatalytic activity. Commercial TiO_2 NPs photocatalytic activity was tested and compared with the biosynthesized TiO_2 NPs. The commercial TiO_2 NPs managed to degrade 84.32% of the MO solution, while the biosynthesized TiO_2 NPs showed a lower degradation percentage except TiO_2-DW-2 and TiO_2-DW-1 with 98.62% and 92.22% of MO degraded, respectively.

The photocatalytic degradation efficiencies of MO initiated by TiO_2 NPs samples are demonstrated in Figure 10(a)-(b), indicating how the degradation rate was significantly fast for TiO_2-DW-2 samples compared to the other samples. Figure 11(a)-(b) are the plots of $\ln(A_0/A_t)$ vs. time (t) of MO degradation in the presence of the biosynthesized TiO_2 NPs. The rate constants of the reactions were determined by the slope calculated from the plots. The plots resulted in regression lines with correlation coefficient (R^2) values (Table 4), which confirm that the reactions fit the first-order kinetic model. The calculated rate constant of TiO_2-DW-2 for MO degradation is 0.0147 min^{-1}

Table 3. The BET surface area and pore volume of the biosynthesized TiO_2 NPs

TiO_2 NPs	S_{BET} (m^2/g)	Average pore size (nm)	Pore volume (cm^3/g)
TiO_2-DW-2	144.0	13.37	0.6602
TiO_2-DW-AA	93.3	10.33	0.3988
TiO_2-EtOH	85.4	18.71	0.4141
TiO_2-EtOH-AA	110.0	9.36	0.3223
TiO_2-Comb	116.0	8.83	0.3335

which is the highest, followed by TiO_2-DW-1 (0.0087 min^{-1}) and TiO_2-Commercial (0.0064 min^{-1}). Table 4 summarizes the rate constant of the biosynthesized and the commercial TiO_2 NPs.

Table 4. Summary of R^2 and pseudo-first-order rate constant of MO degradation in the presence of TiO_2 NPs.

TiO_2 NPs / MO	k (min^{-1})	R^2
TiO_2-Commercial	0.0064	0.9341
TiO_2-DW-1	0.0087	0.8592
TiO_2-DW-2	0.0147	0.8706
TiO_2-DW-5	0.0042	0.9349
TiO_2-DW-10	0.0031	0.9675
TiO_2-DW-15	0.0029	0.9421
TiO_2-DW-AA	0.0023	0.9669
TiO_2-EtOH	0.0030	0.9460
TiO_2-EtOH-AA	0.0029	0.9611
TiO_2-Comb	0.0032	0.9839

4. Conclusion

This study managed to successfully biosynthesize TiO_2 NPs using the leaf extract of *A. indica*. The ethanol and water solvents and acetic acid usage have demonstrated a sizeable influence on the physicochemical properties of the prepared TiO_2 NPs. It was found that the presence/absence of acetic acid in the reaction affects TiO_2 NPs' degree of crystallinity differently based on the solvent used. On the other hand, the particle size is mainly affected by the solvent's polarity, whereby an increase in the polarity leads to a decrease in the size of the NPs. TiO_2-DW-2 showed the highest MO degradation percentage, 98.62% in 270 min, and a pseudo-first-order kinetic constant of MO degradation of 0.0147 min^{-1}. The photocatalytic results demonstrated that TiO_2-DW-2 performed better than commercial TiO_2 under the same test conditions, mainly due to the former's high BET surface area (144.0 m^2/g). Consequently,

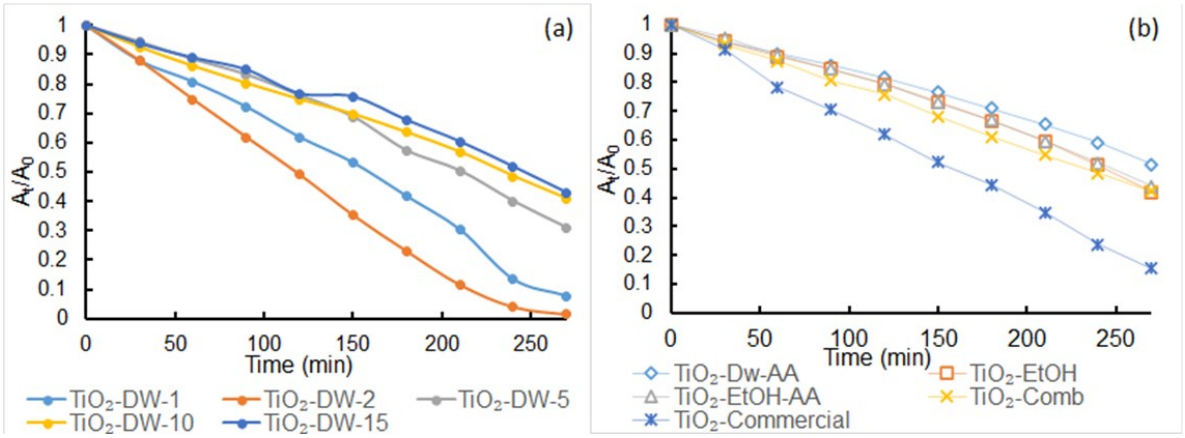

Figure 10. Photodegradation of MO dye solution in the presence of (a) TiO_2-DW-1, TiO_2-DW-2, TiO_2-DW-5, TiO_2-DW-10, and TiO_2-DW-15 and (b) TiO_2-Commercial, TiO_2-DW-AA, TiO_2-EtOH, TiO_2-EtOH-AA, and TiO_2-Comb

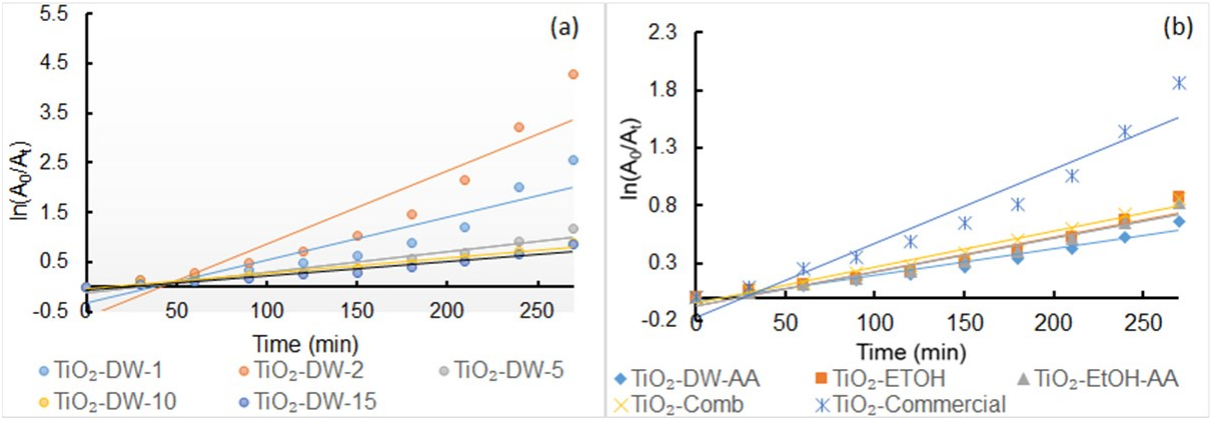

Figure 11. ln (A_0/A_t) vs. t plot for determination of the rate constant for MO degradation using (a) TiO_2-DW-1, TiO_2-DW-2, TiO_2-DW-5, TiO_2-DW-10, and TiO_2-DW-15 and (b) TiO_2-Commercial, TiO_2-DW-AA, TiO_2-EtOH, TiO_2-EtOH-AA, and TiO_2-Comb

based on the TiO_2-DW-2 sample's performance, it can be concluded that this green procedure is highly efficient for the production of TiO_2 NPs with good physicochemical properties and photocatalytic activity with the usage of toxic chemicals kept to a minimum.

Acknowledgement

The authors would like to acknowledge funding from the Ministry of Education (MOE), Malaysia, through Fundamental Research Grant Scheme (FRGS/1/2021/STG04/UTM/02/2) and Universitas Negeri Malang (R.J130000.7354.4B686 PY/2021/00490).

References

[1] Abu-Dalo, M., Jaradat, A., Albiss, B.A., Al-Rawashdeh, N.A.F. (2019). Green Synthesis of TiO_2 NPs/pristine Pomegranate Peel Extract Nanocomposite and its Antimicrobial Activity for Water Disinfection. *J. Environ. Chem. Eng.* 7 (5), 103370. DOI: 10.1016/j.jece.2019.103370.

[2] Al-Rawashdeh, N.A., El-Akhras, A.I., Abbo, M., Al-Mubarak, M.O. (2008). The Effect of Applied Potential on Plasmon Resonance Bands of Nanoscopic Silver Particles Adsorbed on Transparent Electrodes. *Jordan J. Chem.* 3 (1), 57-68.

[3] Venkatasubbu, G.D., Baskar, R., Anusuya, T., Seshan, C.A., Chelliah, R. (2016). Toxicity mechanism of titanium dioxide and zinc oxide nanoparticles against food pathogens. *Colloids Surf. B.* 148 600-606. DOI: 10.1016/j.colsurfb.2016.09.042.

[4] Hasan, I.J., Ab Ghani, M.R., Gan, C.K. (2015). Optimum substation placement and feeder routing using ga-mst. *Appl Mech Mater.* 785, 9-13. DOI: 10.4028/www.scientific.net/AMM.785.9.

[5] Ajmal, N., Saraswat, K., Bakht, M.A., Riadi, Y., Ahsan, M.J., Noushad, M. (2019). Cost-effective and eco-friendly synthesis of titanium dioxide (TiO_2) nanoparticles using fruit's peel agro-waste extracts: Characterization, in vitro antibacterial, antioxidant activities. *Green Chem. Lett. Rev.* 12 (3), 244-254. DOI: 10.1080/17518253.2019.1629641.

[6] Salata, O.V. (2004). Applications of nanoparticles in biology and medicine. *J. Nanobiotechnology.* 2 (1), 3. DOI: 10.1186/1477-3155-2-3.

[7] Saif, S., Tahir, A., Chen, Y. (2016). Green synthesis of iron nanoparticles and their environmental applications and implications. *Nanomaterials.* 6 (11), 209. DOI: 10.3390/nano6110209.

[8] Jemilugba, O.T., Sakho, E.H.M., Parani, S., Mavumengwana, V., Oluwafemi, O.S. (2019). Green synthesis of silver nanoparticles using *combretum erythrophyllum* leaves and its antibacterial activities. *Colloids Interface Sci. Commun.* 31, 100191. DOI: 10.1016/j.colcom.2019.100191.

[9] Chatterjee, A., Nishanthini, D., Sandhiya, Abraham, J. (2016). Biosynthesis of titanium dioxide nanoparticles using vigna radiata. *Asian J. Pharm. Clin. Res.* 9 (4), 85-88.

[10] Fakhari, S., Jamzad, M., and Kabiri Fard, H. (2019). Green synthesis of zinc oxide nanoparticles: A comparison. *Green Chem. Lett. Rev.* 12 (1), 19-24. DOI: 10.1080/17518253.2018.1547925.

[11] Ravichandran, V., Sumitha, S., Ning, C.Y., Xian, O.Y., Kiew Yu, U., Paliwal, N., Shah, S.A.A., Tripathy, M. (2020). Durian waste mediated green synthesis of zinc oxide nanoparticles and evaluation of their antibacterial, antioxidant, cytotoxicity and photocatalytic activity. *Green Chem. Lett. Rev.* 13 (2), 102-116. DOI: 10.1080/17518253.2020.1738562.

[12] Lv, L., Chen, H., Ho, C.T., Sang, S. (2011). Chemical components of the roots of noni (*morinda citrifolia*) and their cytotoxic effects. *Fitoterapia.* 82 (4), 704-708. DOI: 10.1016/j.fitote.2011.02.008.

[13] Lim, S.-L., Goh, Y.-M., Noordin, M.M., Rahman, H.S., Othman, H.H., Abu Bakar, N.A., Mohamed, S. (2016). *Morinda citrifolia* edible leaf extract enhanced immune response against lung cancer. *Food Funct.* 7 (2), 741-751. DOI: 10.1039/C5FO01475A.

[14] Khadar, A., Behara, D.K., Kumar, M.K. (2016). Synthesis and characterization of controlled size TiO_2 nanoparticles via green route using aloe vera extract. *Int. J. Sci. Res.* 5 (1), 1913-1916.

[15] Rufai, Y., Chandren, S., Basar, N. (2020). Influence of solvents' polarity on the physicochemical properties and photocatalytic activity of titania synthesized using *deinbollia Pinnata* leaves. *Front Chem.* 8, 597980. DOI: 10.3389/fchem.2020.597980.

[16] Nadeem, M., Tungmunnithum, D., Hano, C., Abbasi, B.H., Hashmi, S.S., Ahmad, W., Zahir, A. (2018). The current trends in the green syntheses of titanium oxide nanoparticles and their applications. *Green Chem. Lett. Rev.* 11 (4), 492-502. DOI: 10.1080/17518253.2018.1538430.

[17] Singh, J., Dutta, T., Kim, K.-H., Rawat, M., Samddar, P., Kumar, P. (2018). 'Green' synthesis of metals and their oxide nanoparticles: Applications for environmental remediation. *J. Nanobiotechnology.* 16 (1), 84. DOI: 10.1186/s12951-018-0408-4.

[18] Anbalagan, K., Mohanraj, S., Pugalenthi, V. (2015). Rapid phytosynthesis of nano-sized titanium using leaf extract of *azadirachta indica*. *Int. J. Chemtech. Res*. 8 (4), 2047-2052.

[19] Verma, V., Al-Dossari, M., Singh, J., Rawat, M., Kordy, M.G.M., Shaban, M. (2022). A review on green synthesis of TiO_2 NPs: Photocatalysis and antimicrobial applications. *Polymers*. 14 (7), 1444. DOI: 10.3390/polym14071444

[20] Tasbihi, M., Călin, I., Šuligoj, A., Fanetti, M., Lavrenčič Štangar, U. (2017). Photocatalytic degradation of gaseous toluene by using TiO_2 nanoparticles immobilized on fiberglass cloth. *J. Photochem. Photobiol. A*. 336, 89-97. DOI: 10.1016/j.jphotochem.2016.12.025.

[21] Mahshid, S., Askari, M., Ghamsari, M.S. (2007). Synthesis of TiO_2 nanoparticles by hydrolysis and peptization of titanium isopropoxide solution. *J. Mater. Process. Technol.* 189 (1), 296-300. DOI: 10.1016/j.jmatprotec.2007.01.040.

[22] Zhang, B., Asakura, H., Zhang, J., Zhang, J., De, S., Yan, N. (2016). Stabilizing a platinum1 single-atom catalyst on supported phosphomolybdic acid without compromising hydrogenation activity. *Angew. Chem. Int. Ed.* 55 (29), 8319-8323. DOI: 10.1002/anie.201602801.

[23] Garimella, R., Eltorai, A.E.M. (2017). Nanotechnology in Orthopedics. *J. Orthop*. 14 (1), 30-33. DOI: 10.1016/j.jor.2016.10.026.

[24] Jafari, S., Mahyad, B., Hashemzadeh, H., Janfaza, S., Gholikhani, T., Tayebi, L. (2020). Biomedical applications of TiO_2 nanostructures: Recent advances. *Int. J. Nanomedicine*. 15, 3447-3470. DOI: 10.2147/ijn.S249441.

[25] Singh, R., Dutta, S. (2018). A Review on H_2 Production through Photocatalytic Reactions using TiO_2/TiO_2-assisted Catalysts. *Fuel*. 220 607-620. DOI: 10.1016/j.fuel.2018.02.068.

[26] Kumar, S., Muruganandham, T., Jaabir, M. (2014). Original research article decolourization of azo dyes in a two-stage process using novel isolate and advanced oxidation with hydrogen peroxide / hrp system. 3. *Int. J. Curr. Microbiol. Appl. Sci.* 3(1), 514-522.

[27] Khehra, M.S., Saini, H.S., Sharma, D.K., Chadha, B.S., Chimni, S.S. (2005). Decolorization of various azo dyes by bacterial consortium. *Dyes Pigm*. 67 (1), 55-61. DOI: 10.1016/j.dyepig.2004.10.008.

[28] Herrmann, J.M., Duchamp, C., Karkmaz, M., Hoai, B.T., Lachheb, H., Puzenat, E., Guillard, C. (2007). Environmental green chemistry as defined by photocatalysis. *J. Hazard. Mater*. 146 (3), 624-629. DOI: 10.1016/j.jhazmat.2007.04.095.

[29] Zhang, F., Wang, X., Liu, H., Liu, C., Wan, Y., Long, Y., Cai, Z. (2019). Recent advances and applications of semiconductor photocatalytic technology. *Appl. Sci.* 9 (12), DOI: 10.3390/app9122489.

[30] Nabi, G., Raza, W., Tahir, M.B. (2020). Green synthesis of TiO_2 nanoparticle using cinnamon powder extract and the study of optical properties. *J. Inorg. Organomet. Polym*. 30 (4), 1425-1429. DOI: 10.1007/s10904-019-01248-3.

[31] Subhapriya, S., Gomathipriya, P. (2018). Green synthesis of titanium dioxide (TiO_2) nanoparticles by trigonella *foenum-graecum* extract and its antimicrobial properties. *Microb. Pathog*. 116, 215-220. DOI: 10.1016/j.micpath.2018.01.027.

[32] Kaur, H., Kaur, S., Singh, J., Rawat, M., Kumar, S. (2019). Expanding horizon: Green synthesis of TiO_2 nanoparticles using *carica Papaya* Leaves for photocatalysis application. *Mater. Res. Express*. 6 (9), 095-034. DOI: 10.1088/2053-1591/ab2ec5.

[33] Abisharani, J.M., Devikala, S., Kumar, R.D., Arthanareeswari, M., Kamaraj, P. (2019). Green synthesis of TiO_2 nanoparticles using *cucurbita pepo* seeds extract. *Mater. Today*: Proceedings. 14, 302-307. DOI: 10.1016/j.matpr.2019.04.151.

[34] Senthilkumar, S., Rajendran, A. (2018). Biosynthesis of TiO_2 nanoparticles using justicia *Gendarussa* leaves for photocatalytic and toxicity studies. *Res. Chem. Intermed*. 44 (10), 5923-5940. DOI: 10.1007/s11164-018-3464-3.

[35] Pakseresht, S., Cetinkaya, T., Al-Ogaili, A.W.M., Halebi, M., Akbulut, H. (2021). Biologically synthesized TiO_2 nanoparticles and their application as lithium-air battery cathodes. *Ceram. Int.* 47 (3), 3994-4005. DOI: 10.1016/j.ceramint.2020.09.264.

[36] Arabi, N., Kianvash, A., Hajalilou, A., Abouzari-Lotf, E., Abbasi-Chianeh, V. (2020). A facile and green synthetic approach toward fabrication of alcea- and thyme-stabilized TiO_2 nanoparticles for photocatalytic applications. *Arab. J. Chem*. 13 (1), 2132-2141. DOI: 10.1016/j.arabjc.2018.03.014.

[37] Hiremath, S., Antony Raj, M.A.L., Chandra Prabha, M.N., C., Vidya, C. (2018). *Tamarindus indica* mediated biosynthesis of nano TiO_2 and its application in photocatalytic degradation of titan yellow. *J. Environ. Chem. Eng*. 6 (6), 7338-7346. DOI: 10.1016/j.jece.2018.08.052.

[38] Sun, Y., Wang, S., Zheng, J. (2019). Biosynthesis of TiO_2 nanoparticles and their application for treatment of brain injury-an in-vitro toxicity study towards central nervous system. *J. Photochem. Photobiol. B Biol*. 194, 1-5. DOI: 10.1016/j.jphotobiol.2019.02.008.

[39] Elumalai, K., Velmurugan, S. (2015). Green synthesis, characterization and antimicrobial activities of zinc oxide nanoparticles from the leaf extract of *azadirachta indica* (l.). *Appl. Surf. Sci.* 345, 329-336. DOI: 10.1016/j.apsusc.2015.03.176.

[40] Sohail, M.F., Rehman, M., Hussain, S.Z., Huma, Z.-e., Shahnaz, G., Qureshi, O.S., Khalid, Q., Mirza, S., Hussain, I., Webster, T.J. (2020). Green synthesis of zinc oxide nanoparticles by neem extract as multi-facet therapeutic agents. *J. Drug Deliv. Sci. Technol.* 59, 101911. DOI: 10.1016/j.jddst.2020.101911.

[41] Kumar, V.S., Navaratnam, V. (2013). Neem (*azadirachta indica*): Prehistory to contemporary medicinal uses to humankind. *Asian Pac J. Trop. Biomed.* 3 (7), 505-514. DOI: 10.1016/s2221-1691(13)60105-7.

[42] Alzohairy, M.A. (2016). Therapeutics role of *azadirachta indica* (neem) and their active constituents in diseases prevention and treatment. *Evid. Based Complementary Altern. Med.* 2016, 11. DOI: 10.1155/2016/7382506.

[43] Islas, J.F., Acosta, E., G-Buentello, Z., Delgado-Gallegos, J.L., Moreno-Treviño, M.G., Escalante, B., Moreno-Cuevas, J.E. (2020). An overview of neem (*azadirachta indica*) and its potential impact on health. *J. Funct. Foods.* 74, 104171. DOI: 10.1016/j.jff.2020.104171.

[44] Dubey, R.C., Kumar, H., Pandey, R. (2009). Fungitoxic effect of neem extracts on growth and sclerotial survival of macrophomina phaseolina in vitro. *Am. J. Sci.*, 5, 17-24. DOI: 10.7537/marsjas050509.03

[45] Singh, A., Neelam., Kaushik, M. (2019). Physicochemical investigations of zinc oxide nanoparticles synthesized from *azadirachta indica* (neem) leaf extract and their interaction with calf-thymus DNA. *Results Phys.* 13, DOI: 10.1016/j.rinp.2019.102168.

[46] Mankad, M., Patil, G., Patel, D., Patel, P., Patel, A. (2020). Comparative studies of sunlight mediated green synthesis of silver nanoparaticles from *azadirachta indica* leaf extract and its antibacterial effect on *xanthomonas oryzae* pv. *Oryzae. Arab. J. Chem.* 13 (1), 2865-2872. DOI: 10.1016/j.arabjc.2018.07.016.

[47] Thakur, B.K., Kumar, A., Kumar, D. (2019). Green synthesis of titanium dioxide nanoparticles using *azadirachta indica* leaf extract and evaluation of their antibacterial activity. *S. Afr. J. Bot.* 124, 223-227. DOI: 10.1016/j.sajb.2019.05.024.

[48] Vimalkumar, C., Hosagaudar, V., Suja, S., Vilash, V., Krishnakumar, N., Latha, P. (2014). Comparative preliminary phytochemical analysis of ethanolic extracts of leaves of *olea dioica roxb*., infected with the rust fungus *zaghouania oleae* (ej butler) cummins and non-infected plants. *J. Pharmacogn. Phytochem.* 3 (4).

[49] Bouasla, I., Hamel, T., Barour, C., Bouasla, A., Hachouf, M., Bouguerra, O.M., Messarah, M. (2021). Evaluation of solvent influence on phytochemical content and antioxidant activities of two algerian endemic taxa: *Stachys marrubiifolia viv.* and *lamium flexuosum ten.* (*lamiaceae*). *Eur. J. Integr. Med.* 42, 101267. DOI: 10.1016/j.eujim.2020.101267.

[50] Herborne, J. (1973). Phytochemical methods. A guide to modern techniques of plant analysis. 2 5-11. DOI: 10.1007/978-94-009-5921-7

[51] Dash, L., Biswas, R., Ghosh, R., Kaur, V., Banerjee, B., Sen, T., Patil, R.A., Ma, Y.-R., Haldar, K.K. (2020). Fabrication of mesoporous titanium dioxide using azadirachta indica leaves extract towards visible-light-driven photocatalytic dye degradation. *J. Photochem. Photobiol. A.* 400, 112682. DOI: 10.1016/j.jphotochem.2020.112682.

[52] Sarah, R., Tabassum, B., Idrees, N., Hussain, M. (2019) Bioactive compounds isolated from neem tree and their applications. In M. S. Akhtar, M. K. Swamy, & U. R. Sinniah (Eds.), *Natural Bio-active Compounds*: *Production and Applications* (pp. 509-528). Singapore: Springer Singapore. DOI: 10.1007/978-981-13-7154-7_17

[53] Aslam, M., Abdullah, A.Z., Rafatullah, M. (2021). Recent development in the green synthesis of titanium dioxide nanoparticles using plant-based biomolecules for environmental and antimicrobial applications. *J.. Ind. Eng. Chem.* 98, 1-16. DOI: 10.1016/j.jiec.2021.04.010.

[54] Al-Shabib, N.A., Husain, F.M., Qais, F.A., Ahmad, N., Khan, A., Alyousef, A.A., Arshad, M., Noor, S., Khan, J.M., Alam, P., Albalawi, T.H., Shahzad, S.A. (2020). Phyto-mediated synthesis of porous titanium dioxide nanoparticles from *withania somnifera* root extract: Broad-spectrum attenuation of biofilm and cytotoxic properties against hepg2 cell lines. *Front Microbiol.* 11, 1680. DOI: 10.3389/fmicb.2020.01680.

[55] Sankar, R., Dhivya, R., Shivashangari, K.S., Ravikumar, V. (2014). Wound healing activity of *origanum vulgare* engineered titanium dioxide nanoparticles in wistar albino rats. *J. Mater. Sci. Mater. Med.* 25 (7), 1701-1708. DOI: 10.1007/s10856-014-5193-5.

[56] Wang, X., Sø, L., Su, R., Wendt, S., Hald, P., Mamakhel, A., Yang, C., Huang, Y., Iversen, B.B., Besenbacher, F. (2014). The influence of crystallite size and crystallinity of anatase nanoparticles on the photodegradation of phenol. *J. Catal*. 310, 100-108. DOI: 10.1016/j.jcat.2013.04.022.

[57] Chalastara, K., Guo, F., Elouatik, S., Demopoulos, G.P. (2020). Tunable composition aqueous-synthesized mixed-phase TiO_2 nanocrystals for photo-assisted water decontamination: Comparison of anatase, brookite and rutile photocatalysts. *Catalysts*. 10 (4), 407. DOI: 10.3390/catal10040407

[58] Zhang, X., Ge, X., Wang, C. (2009). Synthesis of titania in ethanol/acetic acid mixture solvents: Phase and morphology variations. *Cryst. Growth Des.* 9 (10), 4301-4307. DOI: 10.1021/cg801015b.

[59] Hald, P., Becker, J., Bremholm, M., Pedersen, J.S., Chevallier, J., Iversen, S.B., Iversen, B.B. (2006). Supercritical propanol–water synthesis and comprehensive size characterisation of highly crystalline anatase TiO_2 nanoparticles. *J. Solid State Chem*. 179 (8), 2674-2680. DOI: 10.1016/j.jssc.2006.05.012.

[60] Henderson, M.A. (2011). A surface science perspective on TiO_2 photocatalysis. *Surf. Sci. Rep*. 66 (6), 185-297. DOI: 10.1016/j.surfrep.2011.01.001.

[61] Hussain, M.H., Abu Bakar, N.F., Mustapa, A.N., Low, K.F., Othman, N.H., Adam, F. (2020). Synthesis of various size gold nanoparticles by chemical reduction method with different solvent polarity. *Nanoscale Res. Lett*. 15 (1), 140. DOI: 10.1186/s11671-020-03370-5.

[62] Liu, J., Liang, C., Zhu, X., Lin, Y., Zhang, H., Wu, S. (2016). Understanding the solvent molecules induced spontaneous growth of uncapped tellurium nanoparticles. *Sci. Rep*. 6 (1), 32631. DOI: 10.1038/srep32631.

[63] Tilaki, R.M., Zad, A.I., Mahdavi, S.M. (2007). The effect of liquid environment on size and aggregation of gold nanoparticles prepared by pulsed laser ablation. *J. Nanopart. Res.* 9 (5), 853-860. DOI: 10.1007/s11051-006-9143-0.

[64] Banerjee, I.A., Yu, L., Matsui, H. (2003). Cu nanocrystal growth on peptide nanotubes by biomineralization: Size control of cu nanocrystals by tuning peptide conformation. *Proc. Natl. Acad. Sci. U.S.A.* 100 (25), 14678-82. DOI: 10.1073/pnas.2433456100.

[65] Kumar, P.M., Badrinarayanan, S., Sastry, M. (2000). Nanocrystalline TiO_2 studied by optical, ftir and x-ray photoelectron spectroscopy: Correlation to presence of surface states. *Thin Solid Films*. 358 (1), 122-130. DOI: 10.1016/S0040-6090(99)00722-1.

[66] Zhao, H., Liu, L., Andino, J.M., Li, Y. (2013). Bicrystalline TiO_2 with controllable anatase–brookite phase content for enhanced co_2 photoreduction to fuels. *J. Mater. Chem. A*. 1 (28), 8209-8216. DOI: 10.1039/C3TA11226H.

[67] Phromma, S., Wutikhun, T., Kasamechonchung, P., Eksangsri, T., Sapcharoenkun, C. (2020). Effect of calcination temperature on photocatalytic activity of synthesized TiO_2 nanoparticles via wet ball milling sol-gel method. *Appl. Sci*. 10 (3), 993. DOI: 10.3390/app10030993

[68] Hidalgo, M.C., Aguilar, M., Maicu, M., Navío, J.A., Colón, G. (2007). Hydrothermal preparation of highly photoactive TiO_2 nanoparticles. *Catal. Today*. 129 (1), 50-58. DOI: 10.1016/j.cattod.2007.06.053.

[69] Thommes, M., Kaneko, K., Neimark, A.V., Olivier, J.P., Rodriguez-Reinoso, F., Rouquerol, J., Sing, K.S.W. (2015). Physisorption of gases, with special reference to the evaluation of surface area and pore size distribution (iupac technical report). *Pure Appl. Chem*. 87 (9-10), 1051-1069. DOI: 10.1515/pac-2014-1117.

[70] Al-Othman, Z.A. (2012). A review: Fundamental aspects of silicate mesoporous materials. *Materials*. 5 (12), 2874-2902. DOI: 10.3390/ma5122874.

[71] Mahmoud, H.A., Narasimharao, K., Ali, T.T., Khalil, K.M.S. (2018). Acidic peptizing agent effect on anatase-rutile ratio and photocatalytic performance of TiO_2 nanoparticles. *Nanoscale Res. Lett*. 13 (1), 48. DOI: 10.1186/s11671-018-2465-x.

[72] Nguyen, T., Hwang, M.J., Lee, S.-S., Choe, D.-E., Ryu, K.S. (2010). Characterization of TiO_2 synthesized in acidic conditions at low temperature by sol-gel method. *J. Korean Inst. Met. Mater.* 17, 409-414. DOI: 10.4150/KPMI.2010.17.5.409.

[73] Kim, D.S., Kwak, S.-Y. (2007). The hydrothermal synthesis of mesoporous TiO_2 with high crystallinity, thermal stability, large surface area, and enhanced photocatalytic activity. *Appl. Catal. A: Gen*. 323, 110-118. DOI: 10.1016/j.apcata.2007.02.010.

[74] Li, W., Wu, Z., Wang, J., Elzatahry, A.A., Zhao, D. (2014). A perspective on mesoporous TiO_2 materials. *Chem. Mater*. 26 (1), 287-298. DOI: 10.1021/cm4014859.

[75] Azeez, F., Al-Hetlani, E., Arafa, M., Abdelmonem, Y., Nazeer, A.A., Amin, M.O., Madkour, M. (2018). The effect of surface charge on photocatalytic degradation of methylene blue dye using chargeable titania nanoparticles. *Sci. Rep*. 8 (1), 7104. DOI: 10.1038/s41598-018-25673-5.